



Original article

Structural, optical, morphological, sun-light driven photocatalytic and antimicrobial investigations of Ag₂S and Cu/Ag₂S nanoparticles

Nouf M. Al-Enazi

Department of Biology, College of Science and Humanities in Al-Kharj, Prince Sattam Bin Abdulaziz University, Al-Kharj 11942, Saudi Arabia

ARTICLE INFO

Keywords:

Silver sulphide
Photocatalysis
Well diffusion method
Antimicrobial activity
Wastewater treatment

ABSTRACT

This study focusses on the preparation of silver sulphide (Ag₂S) and Cu-doped Ag₂S (Cu/Ag₂S) nanoparticles (NPs) by sol-gel method and demonstrated their photocatalytic and antibacterial applications. The X-ray diffraction (XRD) and Fourier-transform infrared (FTIR) analysis demonstrated that the prepared NPs are effectively crystallized in the polycrystalline single-phase monoclinic geometry of Ag₂S. The optical bandgap is significantly reduced, and for both the sample the average grain size is observed to have narrowed from 42 nm to 23 nm. Both NPs were confirmed to be spherical nature as observed by scanning electron microscopy (SEM), and the energy dispersive X-ray (EDX) spectroscopy analysis validated the presence of all necessary components at the expected concentrations in the obtained samples. Under the irradiation of sunshine, the photocatalytic properties of each sample were investigated for their ability to facilitate the photodegradation of a hazardous methylene blue (MB) dye in an aqueous solution. Cu/Ag₂S sample possesses a profound photocatalytic reaction for the destruction of MB dye. Furthermore, the Cu-doped Ag₂S NPs suppress the proliferation of *Staphylococcus aureus* and *Escherichia coli*. In comparison to pure Ag₂S NPs, Cu/Ag₂S showed enhanced antibacterial activity against both the bacteria. Current study suggests that the Cu doped Ag₂S NPs could be a promising material for wastewater treatment and antimicrobial agents.

1. Introduction

Nanotechnology and the exploration of nanomaterials have emerged as a rapidly evolving field with immense potential for various applications in diverse sectors, including medicine, energy, and environmental science (Tang and Zheng, 2018; Sathishkumar et al., 2016; Jesion et al., 2015). From the various NPs, silver sulfide (Ag₂S) NPs has garnered significant importance because of their one-of-a-kind qualities and numerous uses. Recently, researchers have explored the incorporation of copper (Cu) into Ag₂S NPs, aiming to enhance their antimicrobial and photocatalytic activities (Ameen et al., 2023c; Fernández et al., 2010). This research delves into the intricate characteristics and multifaceted applications of Ag₂S and Cu/Ag₂S NPs, shedding light on their structural composition, optical properties, and morphological attributes, as well as their potential in two pivotal domains – photocatalysis under sunlight and antimicrobial activities. Also, it provides the antibacterial and photocatalytic potentials of Ag₂S NPs and the benefits of Cu doping in achieving advanced functionalities. The development of germs that are resistant to antibiotics has emerged as a major worry on a global scale,

necessitating the development of alternative antibacterial strategies. Ag₂S NPs have demonstrated remarkable antibacterial properties, owing to their ability to release silver ions (Ag⁺) upon contact with biological systems. The released Ag⁺ ions exhibit potent antimicrobial effects by disrupting bacterial cell membranes, inhibiting vital enzymes, and causing oxidative stress. As a consequence of this, Ag₂S nanoparticles have shown bactericidal activity (Jyoti et al., 2016; Thirunavoukarasu et al., 2013).

The practice of photocatalysis, which uses light energy to drive chemical reactions, has attracted a lot of interest in environmental remediation and renewable energy (Pandurangan and Kim, 2015). Ag₂S NPs possess excellent photocatalytic properties due to their narrow bandgap, which enables the captivation of visible light (Atmani et al. 2010; Pasukphun et al. 2010). When illuminated, Ag₂S NPs can generate electron-hole pairs, initiating redox reactions with organic pollutants, heavy metals, and other contaminants. This photocatalytic activity leads to the degradation of harmful substances and the conversion of pollutants into less toxic compounds, promoting environmental sustainability (Parthipan et al. 2021; Elayaraja et al. 2020; Rajeshwar et al. 2008). To

Peer review under responsibility of King Saud University.

E-mail address: n.alenazi@psau.edu.sa.<https://doi.org/10.1016/j.sjbs.2023.103840>

Received 2 September 2023; Received in revised form 26 September 2023; Accepted 15 October 2023

Available online 18 October 2023

1319-562X/© 2023 The Author(s). Published by Elsevier B.V. on behalf of King Saud University. This is an open access article under the CC BY-NC-ND license (<http://creativecommons.org/licenses/by-nc-nd/4.0/>).

further improve the photocatalytic and antibacterial activity of Ag₂S NPs, researchers doped NPs with copper (Cu) ions. Cu doping introduces additional functionalities and synergistic effects, leading to improved performance. Cu ions can augment the release of Ag⁺ ions, thereby enhancing the bactericidal effects (Ahmed et al. 2018; Qian et al. 2001). Moreover, Cu doping modifies the electronic band structure of Ag₂S NPs, extending their absorption range to the visible and near-infrared regions, thereby enhancing the photocatalytic efficiency. Additionally, Cu imparts enhanced stability and durability to the NPs, ensuring long-term performance in various applications (Thirumala Rao et al. 2015; Chauhan et al. 2014; Mittal et al. 2014).

Recent years, transition metal (TM) doped Ag₂S semiconductors have been majorly studied because of their broad utilization in biomedical and environmental fields. Among many TM-based compounds, Due to its exceptional electrical conductivity, high reactivity in the visible region and high solubility of the Cu atoms in the Ag₂S matrix, Cu-doped Ag₂S is a particularly appealing material. Fakhri et al. reported the antimicrobial activity of Cu-doped Ag₂S NPs against pathogenic bacteria. The results demonstrate the bactericidal effect of Ag₂S NPs because of the delivery of silver ions, leading to cell membrane disruption and inhibition of bacterial evolution (Fakhri et al., 2015). Liu et al. shows the visible light guided catalytic properties of RGO/Ag₂S/TiO₂ ternary heterojunctions for environmental remediation. The study highlights the ability of Ag₂S NPs to degrade organic impurities in the existence of visible light, making them suitable for polluted water treatment and air sanctification (Liu et al., 2017). Okla et al. investigates the synergistic effects of 3D CdS-Ag₂S nanospheres and light on the antibacterial and photocatalytic activities (Okla et al., 2022). Hence, Cu-doped silver sulfide nanoparticles hold great promise for sun-light driven photocatalytic and antimicrobial investigations due to their enhanced photocatalytic activity, visible light responsiveness, antimicrobial properties, sustainability, and versatility. These nanoparticles have the potential to address environmental and health-related challenges while harnessing the abundant and renewable energy source of sunlight. The combination of copper and silver in these nanoparticles can lead to synergistic effects, where the properties of the two elements complement each other, resulting in improved performance (Ameen, 2022).

In this direction, the present investigations focus on the sol-gel preparation of Ag₂S and Cu-doped Ag₂S NPs and its application in photocatalysis and combating bacteria. The study highlights the potential of these NPs in addressing the issues of antibiotic resistance, which are major concerns in healthcare and the environment. The results demonstrate the significant antibacterial of the Cu/Ag₂S NPs, as well as their high photocatalytic efficiency in degrading organic pollutants with good recyclability and stability under sunlight irradiation.

2. Experiments

2.1. Materials

To prepare the pure and copper-doped silver sulphide NPs; silver nitrate monohydrate (AgNO₃·H₂O), copper nitrate monohydrate (Cu(NO₃)₂·H₂O), sodium sulphide (Na₂S) and N-Methyl-2-pyrrolidone (NMP) obtained from Sigma-Aldrich. Bacteria strains used in this study was generously provided by the microbiology department located in our university.

2.2. Synthesis

A sol-gel synthesis technique was utilized for the preparation of the pure Ag₂S and 10 % Cu-doped Ag₂S (Cu/Ag₂S) NPs. To synthesize pure Ag₂S NPs, 20 mL of 1.950 g of Na₂S aqueous solution was added drop by drop to 60 mL of 8.491 g Ag(NO₃)₃ solution at 70 °C with vigorous stirring. After adding 20 mL NMP and the solution temperature is raised to 80 °C and maintained for 4 h to obtain a blackish thick gel. This

resultant gel was cleaned multiple times with distilled water and ethanol separately along with their mixture. After drying in an oven set to 70°, the wet precipitate was then ground up for 20 min and calcined for 2 h at the temperature of 400 °C to eliminate volatile impurities and increase the crystallinity. Finally, the sample was reground for 30 min for homogeneity of the material (Kumari et al., 2014).

Further, for the synthesis of Cu/Ag₂SNPs: both 8.067 g of AgNO₃, and 0.603 g of Cu(NO₃)₂ were completely dissolved in 60 mL doubly ionised distilled water, and 1.951 g of Na₂S in 20 mL distilled water was prepared separately to achieve the aqueous solution. 20 mL solution of Na₂S was added dropwise to 60 mL solution of Ag(NO₃)₃ and Cu(NO₃)₂ at 70 °C and mixed with 20 mL NMP solution. The magnetic stirring of this solution at 80 °C for 4 h produced a blackish-thick gel. This thick gel was washed with water and ethanol and dried at 70 °C for 20 min. The final power was reground for 30 min after calcining at 400 °C for 2 h (Kumari et al., 2014).

2.3. Photocatalytic activity

Under sunlight, the utilisation of synthesised NPs for the degradation of MB dye was studied. The catalyst was typically tested after being suspended in a 100 mL MB dye solution containing 10 mg/L and expose to sunlight. The aliquots of the reaction mixture were analysed at various intervening times throughout 180 min. Using absorption spectrophotometer, the MB dye concentration in samples was determined.

2.4. Antibacterial activity and minimal inhibitory concentration (MIC)

Typically, 100 µL bacterial suspensions were evenly spread across culture agar plates. Following this, 100 µL of NPs were introduced into wells created in the plates and incubated at a temperature of 37 °C for 24 h. Distilled water was used as a control in this experiment. After the initial period of incubation, the diameter of the zone formed around the well was noted as the zone of inhibition (ZOI), which corresponds to bacterial growth inhibition. A broth-dilution method was employed to quantify the MIC of NPs required to exhibit antibacterial activity. The inoculums of bacteria were diluted sufficiently to reach 10⁶ CFU/mL. Bacteria were cultured for 24 h at 37 °C in various NPs concentrations and treated with 20 µL of triphenyltetrazolium chloride (3 mg/mL). After storing at 20 min at room temperature, the bacterial proliferation was visually assessed through a noticeable change in colour to pink. The lowest concentration measured at which no observable colour change signalled the lack of metabolically active cells was recorded as MIC.

2.5. Characterizations

Spectra of FTIR obtained using a Perkin Elmer spectrophotometers (spectrum-2) were used to estimate bonds and functional groups. Scanning electron microscopy (JEOL JSM-6510 LV) was utilized to study the surface characteristics of the samples, and the EDX spectra for elemental composition. The Lambda-950 UV-Vis spectrophotometer (Perkin Elmer) was used to evaluate the optical properties, and the band gap.

3. Results

3.1. Structural analysis

The crystallographic structure was investigated using XRD data (Shimadzu LabX XRD-6100 x-ray diffractometer) for both Ag₂S and Cu/Ag₂S powder NPs as shown in Fig. 1 (a, b). After scanning the diffraction pattern from 20° to 80°, numerous notable peaks appeared within the selected range. The prominent diffraction peaks are observed at 26°, 29°, 31.5°, 33.8°, 34.5°, 36.7°, 38°, 40.8°, 43.4°, 44.5°, 46.3°, 48.5°, 53.3°, 58.2°, and 64° in pure Ag₂S sample, attribute to the respective (-101), (111), (-112), (120), (-121), (121), (-103), (031),

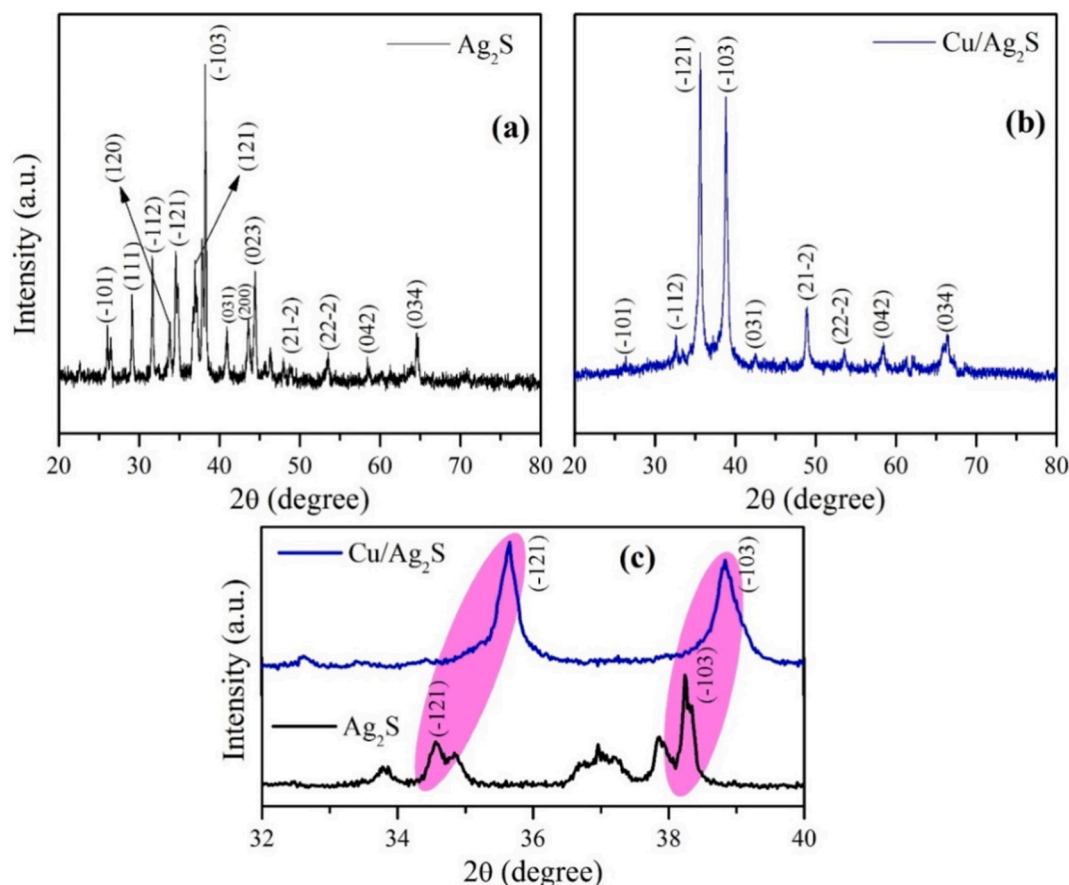


Fig. 1. The typical XRD spectra of Ag_2S (a) and $\text{Cu}/\text{Ag}_2\text{S}$ (b), peak shifting behaviour of plane (-121) and (-103) (c).

(200), (023), (113), (21-2), (22-2), (042) and (034) planes, belonging to the presence of monoclinic Ag_2S crystal structure phase. The lattice parameters, $a = 4.219 \text{ \AA}$ and $c = 7.852 \text{ \AA}$ as matched with the ICDD-JCPDS file number: 00-014-0072 (Hamed et al., 2020). While Cu-doped Ag_2S sample has (-101) , (-112) , (-121) , (-103) , (031), (21-2), (22-2), (042) and (034) Miller planes at their respective 2θ values. The Ag_2S phase purity in the Cu-doped Ag_2S sample can be described based on the lack of any diffraction peak associated with copper oxide phases. The lattice parameters for $\text{Cu}/\text{Ag}_2\text{S}$ were $a = 4.208 \text{ \AA}$ and $c = 7.841 \text{ \AA}$ for $\text{Cu}/\text{Ag}_2\text{S}$. As obtained from Fig. 1 (c), the breadth of the most intense plane peak (-103) is somewhat wider and displaced for higher 2θ values for $\text{Cu}/\text{Ag}_2\text{S}$, which can be ascribed to the fact that the lattice parameters and crystallite size have decreased. The average crystallite/grain size is evaluated from XRD peaks using the Debye-Scherrer equation to be 42 nm and 23 nm for pure Ag_2S and Cu-doped Ag_2S NPs, respectively.

Fig. 2 shows the FTIR spectra of both Ag_2S and $\text{Cu}/\text{Ag}_2\text{S}$ NPs, which were performed between 400 and 4000 cm^{-1} . It was determined that there are distinct stretching bands that correlate to distinct stretching classes. The band that is located at 1100 cm^{-1} in each of the samples reflects C = O group presence. The band at 2360 cm^{-1} account for the Ag-S bonds in manufactured Ag_2S . The findings from the IR study are in good accord with previous findings that were done by Pernia et al. (Pernia et al., 2014), as well as with the values that are considered to be standard in the literature. The preparation of cysteine-assisted silver sulfide NPs has been confirmed by the detection of an essentially identical peak at 2300 cm^{-1} by Pernia et al. The high surface-to-volume ratio of nanocrystalline materials may allow taking moisture and generating a broad absorption peak of O-H stretching bond at about 3430 cm^{-1} . This peak is caused by the water molecules that have been absorbed by the material. In addition, the spectra of $\text{Cu}/\text{Ag}_2\text{S}$ exhibit a prominent peak at

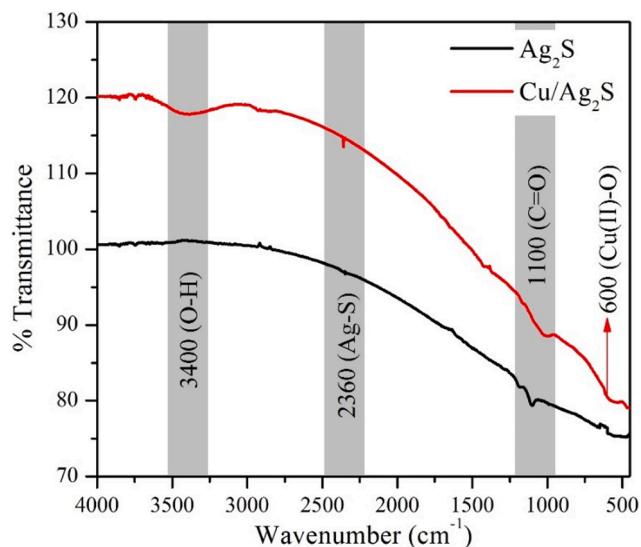


Fig. 2. FTIR spectra of Ag_2S and $\text{Cu}/\text{Ag}_2\text{S}$ nanoparticles.

600 cm^{-1} , which is typical of Cu-O bond formation, and can be found in the spectrum (Banerjee et al., 2016).

3.2. Morphological analysis

The image acquired from SEM revealed the irregular-sized spherical NPs of Ag_2S as shown in Fig. 3(a). Cu-doped Ag_2S material shows the same morphology, but contains some specific agglomeration of NPs

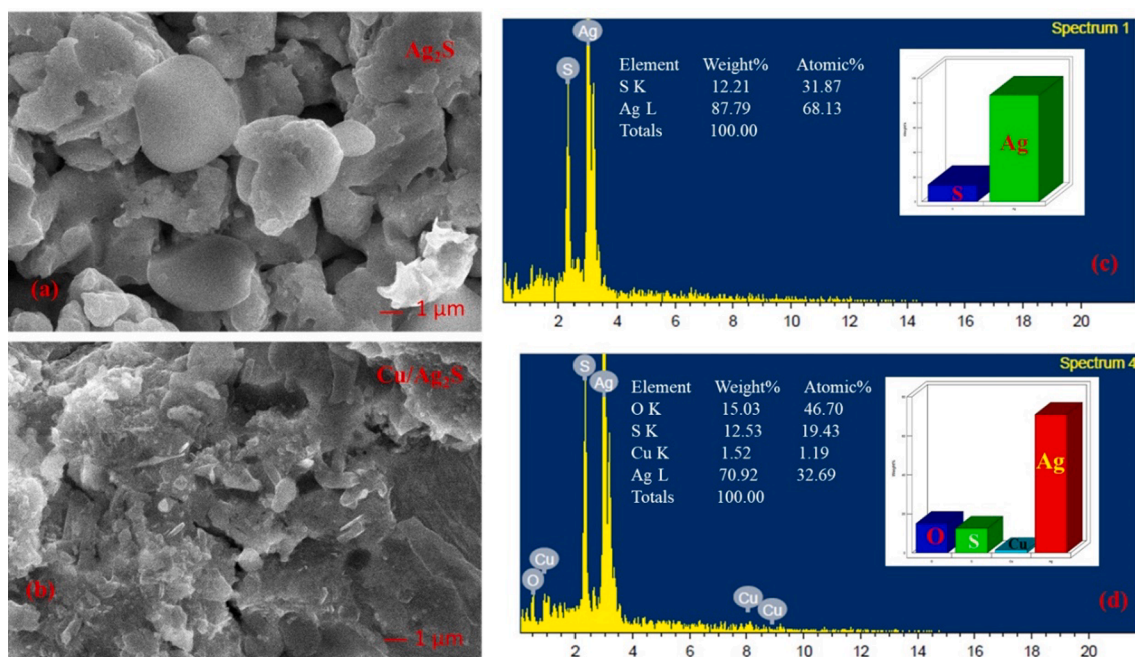


Fig. 3. Illustrate the SEM micrographs of (a) Ag₂S, (b) Cu/Ag₂S and EDX spectra of (c) Ag₂S, (d) Cu/Ag₂S.

(Fig. 3(b)). The observed particle size of Cu/Ag₂S is smaller than that of pure Ag₂S NPs as can be seen in the micrograph. In addition, the EDX spectra as depicted in Fig. 3(c) and (d) were analyzed, which demonstrated that the Ag₂S NPs contain the elemental components of both Ag and S and Ag, S & O in Cu/Ag₂S NPs, respectively. The elemental compositions are presented in the table format as atomic % and weight % together with individual elements bar graphs (Fig. 3c and 3d).

3.3. Optical analysis

The absorption peaks may be seen for Ag₂S at around 328 nm and 508 nm, with a minor red-shift visible in the spectra of Cu/Ag₂S samples that follow one another, as shown in Fig. 4(a). The Tauc plot, which can be shown in Fig. 4(b) is utilized to calculate the band gap energy. The band gap estimated for Ag₂S and Cu/Ag₂S individual samples was 1.88 eV and 1.79 eV, respectively. The finding demonstrates that the energy band gap has been narrowing.

3.4. Applications

3.4.1. Photocatalytic activity

Fig. 5 (a, b) shows the absorbance spectra for the photocatalytic disintegration of MB dye solution, which have been measured on UV-Vis spectrophotometer using Ag₂S and Cu/Ag₂S NPs photocatalysts under sunlight irradiation and the following experimental conditions were: pH 7, 100 ppm MB dye, and 30 mg photocatalyst weight. First, the absorption spectra were taken for dark (30 min) and for sunlight exposure at different time intervals from 30 to 180 min. A small degradation has been obtained in the dark due to the adsorption of MB dye at 663 nm by both samples. When reactive radicals are available, this type of photocatalyst can be used to degrade all MB dye. The photocatalyst is easily recovered from the solution once the MB dye has been destroyed via centrifugation.

Fig. 6 (a and b) show the C/C₀ and % MB degradation for both synthesized samples, respectively. With Ag₂S and Cu/Ag₂S, the MB dye removal efficiency is found to be 40 % and 84 % in 180 min under the exposure to sunlight. The finding suggests that the doping of Cu in Ag₂S

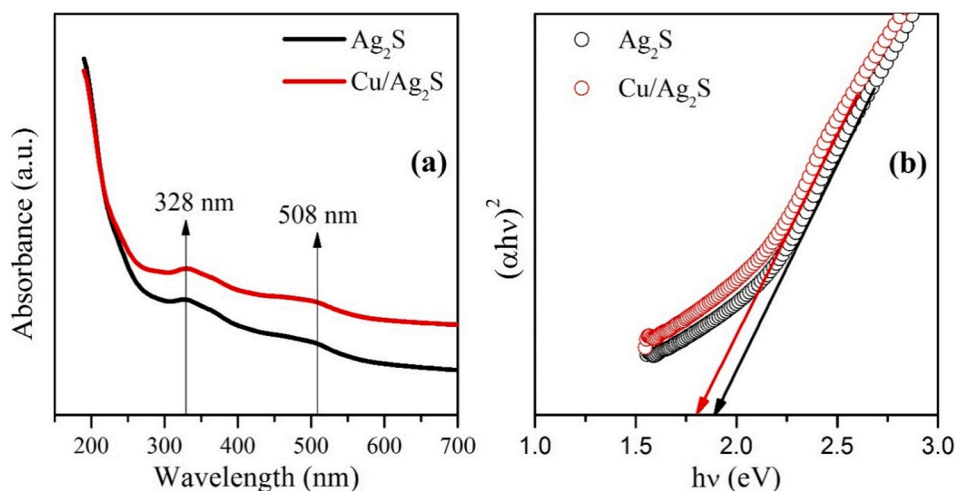


Fig. 4. The absorbance spectra (a) and Tauc plot (b) of Ag₂S and Cu/Ag₂S.

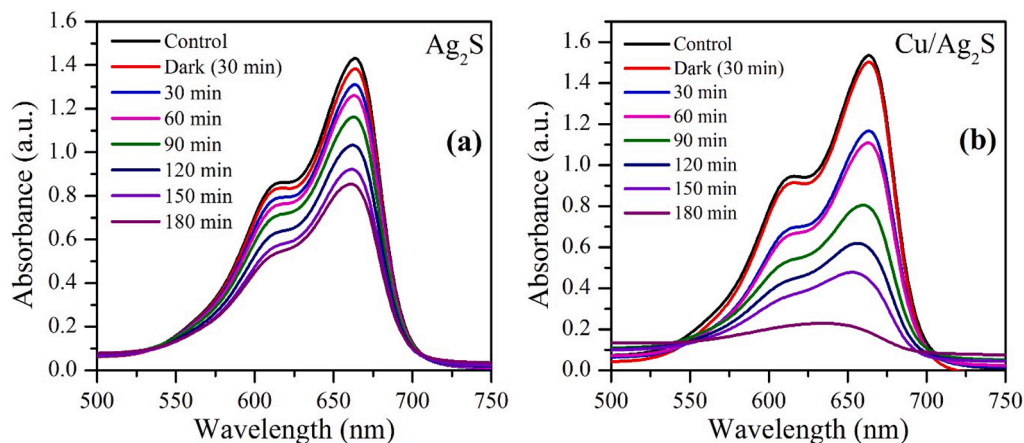


Fig. 5. Absorbance spectra at different time intervals to measure the remaining MB concentration in the solution under sunlight irradiation for (a) Ag₂S and (b) Cu/Ag₂S nanoparticles.

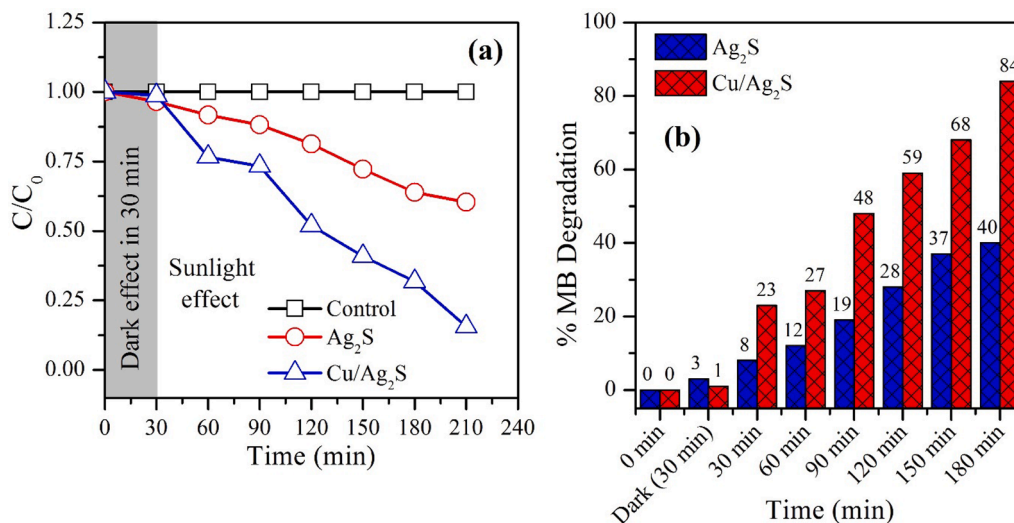


Fig. 6. Shows (a) the variation of C/C₀ with time for Ag₂S and Cu/Ag₂S in the dark (for 30 min) as well as in sunlight (0–180 min), (b) % Degradation of MB dye for Ag₂S and Cu/Ag₂S nanoparticles.

increases the light driven catalytic activity. The following may account for the enhanced light driven photocatalytic activity seen in the presence of Cu: (i) larger oxygen vacancy slowing their combination of electron-hole pair concentrations, which operate as energy traps, and (ii) the

resulted emergence of generalized localized states enhance the absorption of photon (Anandan and Rajendran, 2015; Khan et al., 2023b). Here, the % degradation of MB was calculated from equation (1) (Khan et al., 2023b),

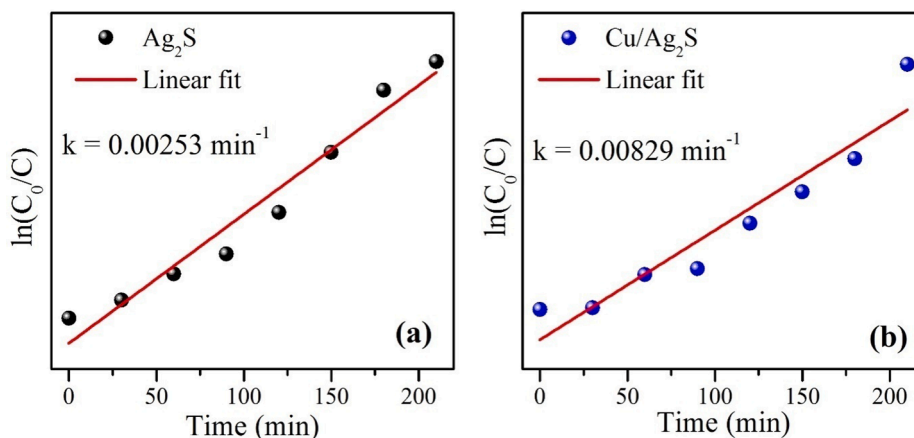


Fig. 7. Photocatalytic degradation of MB dye for Ag₂S NPs (a), and Cu/Ag₂S NPs (b). Analysed by the first-order rate equation to determine, k.

$$\% \text{Degradation of MB dye} = \frac{C_0 - C_t}{C_0} \times 100 \quad (1)$$

Where, C_0 and C_t represent the MB concentration at 0 min and 180 min, respectively, before and after deterioration. Fig. 7 shows the reaction rate constant (k) for the removal of MB dye with photocatalyst Ag_2S and Cu-doped Ag_2S , which is calculated using the rate kinetics (pseudo-first order) equation (2) (Khan et al., 2023b),

$$\ln\left(\frac{C_0}{C_t}\right) = kt \quad (2)$$

The reaction rate constant k using the above equation was found to be 0.0025 min^{-1} and 0.0083 min^{-1} for Ag_2S and $\text{Cu}/\text{Ag}_2\text{S}$, respectively.

3.4.2. Antimicrobial activity

The antimicrobial property of the NPs was evaluated utilizing the agar well diffusion method (Fig. 9) in comparison to the control (H_2O). The zone of inhibition (ZOI) analysis was used to assess the extent of bacterial growth inhibition. In the control group, no inhibition of bacterial growth was observed. However, it is noteworthy that both NPs demonstrated significant bacterial growth inhibition, as evidenced by the presence of clear ZOI surrounding the wells.

The MIC was determined through serial dilution to determine the lowest dose of antibacterial agent that successfully halted bacterial growth. According to Table 1, the MIC values for Ag_2S against the pathogens ranged between 10 and 15 $\mu\text{g}/\text{mL}$, while for $\text{Cu}/\text{Ag}_2\text{S}$, they varied from 5 to 10 $\mu\text{g}/\text{mL}$.

4. Discussion

The XRD spectra of both the NPs such as Ag_2S and $\text{Cu}/\text{Ag}_2\text{S}$, as displayed in Fig. 1(a, b). This slight decrement in the values of the lattice constant may arise because of the incorporation of Cu atoms in the matrix of Ag_2S NPs. Additionally, the smallest variance in a may be because of the local disorder in the lattice as well as the presence of empty sites in the lattice. However, Cu doping alters the grain size of the Ag_2S . The substitutional insertion of copper into the Ag_2S lattice is established by the shift in peak location, peak intensity, D-value, and lattice parameter. Also, no band present corresponding to C-S bond stretching suggests that this bond has been completely severed by the reaction process that was described earlier and has resulted in the production of Ag_2S (Fig. 2) (Khan et al., 2023b, 2021).

To evaluate the surface morphology and elemental composition of Ag_2S and $\text{Cu}/\text{Ag}_2\text{S}$, respectively, SEM and EDX analyses were performed. The image from the SEM revealed irregularly sized spherical NPs, as represented in Fig. 3 (a, b). The absence of any contaminating materials in the samples demonstrates the purity of this method (Fig. 3 (c, d)) (Akhter et al., 2020; Binjawhar et al., 2023).

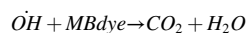
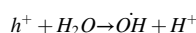
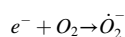
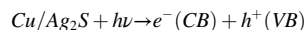
The absorbance mode of the UV-Vis spectra was used for both the samples, and the results show that the distinct characteristic peaks are present for Ag_2S and $\text{Cu}/\text{Ag}_2\text{S}$. This indicates that the samples do not contain any impurity phases as shown in Fig. 4(a). The reactive oxygen species (ROS) production under the influence of visual electromagnetic radiation is closely related to the result of band gap narrowing, as determined using the Tauc plot (Fig. 4b) (Podporska-Carroll et al., 2017).

Table 1

Zone of inhibition (ZOI) and minimum inhibitory concentration (MIC) of *E. coli* and *S. aureus*.

Bacterial culture	ZOI (mm)		MIC ($\mu\text{g}/\text{mL}$)	
	Ag_2S	$\text{Cu}/\text{Ag}_2\text{S}$	Ag_2S	$\text{Cu}/\text{Ag}_2\text{S}$
<i>E. coli</i>	11.00 ± 0.50	13.50 ± 0.50	10	5
<i>S. aureus</i>	10.50 ± 1.00	17.25 ± 0.25	15	10

In wastewater treatment, both Ag_2S and $\text{Cu}/\text{Ag}_2\text{S}$ NPs have been shown to have a lot of photocatalytic activity. In photocatalysis, a catalyst (Ag_2S and $\text{Cu}/\text{Ag}_2\text{S}$ in this case) uses light energy to speed up a chemical reaction. Photocatalysis can be used to get rid of organic pollutants and other pollutants from water as part of the cleaning of wastewater. Photocatalysts like these NPs because they have unique qualities like a large surface area, a lot of active sites, and the ability to absorb light well. Because $\text{Cu}/\text{Ag}_2\text{S}$ NPs has the ability to absorb both UV-visible lights, this could speed up a wide range of chemical processes. The direct absorption of supra-band gap photons, as well as the formation of electron-hole pairs in semiconductor particles, is the first stages in the photocatalytic process of semiconductors. The charge carriers are subsequently transported to the particle's surface via a process known as diffusion. The following are the photocatalytic reactions i.e. involved in this study,



Peroxide ($\dot{\text{O}}_2^-$) and hydroxyl radicals ($\dot{\text{O}}\text{H}$), which are very reactive, are thought to be responsible for the photocatalytic effect. On the surface of water, electrons and holes create hydroxyl radicals ($\dot{\text{O}}\text{H}$). It is possible that, if there are interface imperfection states, it will be capable of capturing the electrons or holes, which will prevent recombination and may cause the pace of redox processes to increase (Ameen et al., 2023b). In this instance, Cu acted as an electron collector and enhances the photocatalytic activity rate. It is known that photocatalytic activity is dependent on crystal quality, morphology and surface area and that it can be enlarged by decelerating the reattach of photon-induced electron-hole pairs, raising the number of surface-adsorbed reactant varieties while simultaneously extending the wavelength of the excitation to a region of energy that is lower. This photocatalyst stands out because it is stable and can be recycled, which are both important qualities. The stability and recyclability of the photocatalyst ($\text{Cu}/\text{Ag}_2\text{S}$) were studied by breaking down the same amount of dye three times with the same amount of photocatalyst. As shown in Fig. 8, there is no alteration in how well the photocatalyst works. The pollution (MB dye) breaks down at the same rate, and there is no sign of the photocatalyst breaking down (Ahmed et al., 2013; Zhang et al., 2011).

In the case of the antimicrobial activity of both NPs, the NPs have

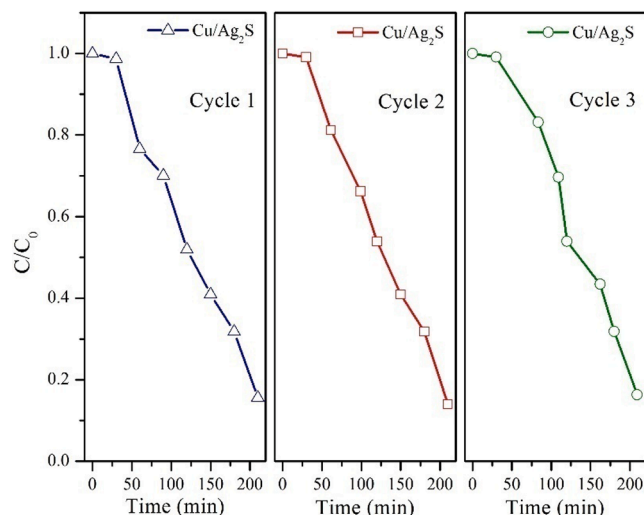


Fig. 8. The recyclability and stability of $\text{Cu}/\text{Ag}_2\text{S}$ NPs photocatalyst.

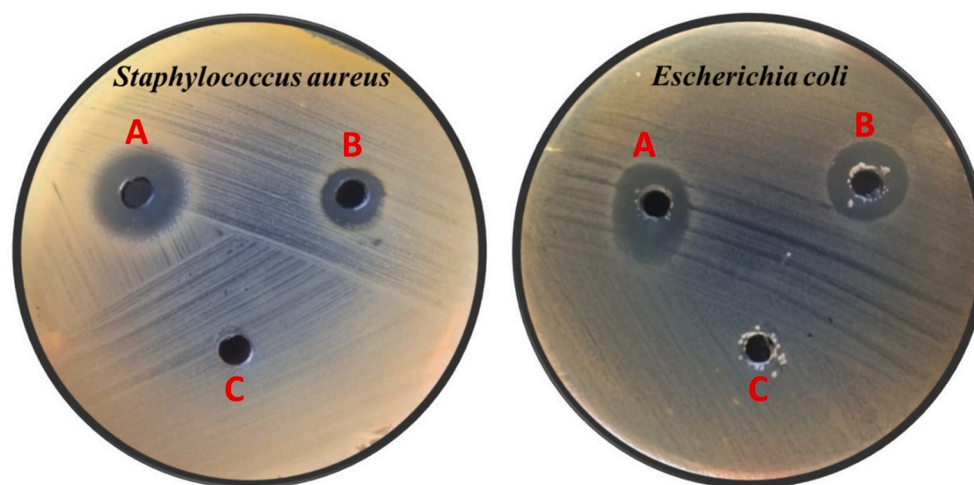


Fig. 9. Well diffusion method for antimicrobial activity for(A) Cu/Ag₂S NPs, (B) Ag₂S NPs, and(C) control (H₂O).

been connected to a variety of distinct pathways, any of which may be responsible for their bactericidal effect. The existence of a charged group in the pure and Cu-doped Ag₂S NPs, as well as the likelihood that electrostatic forces come into play when NPs attach to the bacterial membranes, may both be accountable for the NPs antibacterial properties (Ameen et al., 2023a; Stoimenov et al., 2002). It can be explained by considering the NPs first attached to the bacterial membranes making a hole in the cell and releasing the cell's contents to leak out and a lot of ROS to be made, which messed with important functional groups like thiol and stopped the bacteria from reproducing (Baker and Satish, 2012; Khan et al., 2023a).

Both the NPs release Ag²⁺/Ag¹⁺ and Cu²⁺ ions, which, as a result of electrostatic attraction, collide with the negatively surface charged bacterial cell wall and disintegrate the bacteria's protective cell wall (Al-Enazi et al., 2023; Ameen et al., 2023d). Consequently, the material found inside the cell will be exposed. In a similar vein, the bactericidal effect of NPs such as Ag₂S and Cu/Ag₂S can be linked to the production of hydrogen peroxide by Ag₂S. Hydrogen peroxide is a powerful bacterial growth inhibitor and is responsible for the NP's bactericidal properties (Sawai and Yoshikawa, 2004). According to Lin *et al.*'s explanation (Pal et al., 2007), the ions of Ag atoms that are produced by the nanocomposites are stated to have antibacterial capabilities that are broad in scope. Particularly, when Cu-based Ag₂S NPs interact with bacterial cells, an increase in the bactericidal activity of the Ag₂S NPs is seen. Doping the matrix of Ag₂S NPs with Cu atoms has the effect of improving the electron-hole charge dissociation by reducing the bandgap energy. As a result, additional coalescence is delayed, which boosts the antibacterial activity (Ameen and Majrashi, 2023; Khan et al., 2023a, 2020).

5. Conclusion

The high-performance antimicrobial and photocatalytic agents Cu-doped Ag₂S NPs were processed by using the cost-effective sol-gel method. The single-phase monoclinic structure of both the NPs has been verified by XRD and FTIR, and probable impurities that are commonly observed were not obtained in the sample. Cu inclusion resulted in a decrease in average crystallite size, which could be attributed to the lower ionic radius of Cu²⁺ compared to Ag¹⁺ cation. The FT-IR spectroscopy signified the existence of Ag-S/Cu-O bonding and O-H stretching vibrations due to moisture. The images obtained SEM showed spherical shape NPs with some agglomeration. Ag₂S and Cu/Ag₂S optical band gaps were observed to range from 1.88 eV to 1.79 eV, respectively. Slow recombination rate of e⁻/h⁺ pairs is better for photocatalytic degradation of MB and antimicrobial activity. The

photocatalytic activity of Cu/Ag₂S NPs is found to be better as compared to the pure Ag₂S NPs. The value of *k* is calculated as 0.00253 min⁻¹ and 0.00829 min⁻¹ for Ag₂S and Cu/Ag₂S samples, which can break down MB dye in wastewater by up to 40 % and 84 %, respectively. The study suggests that the Ag₂S Cu/Ag₂S NPs offer a promising avenue for advanced applications in antimicrobial and photocatalytic domains. Their unique properties, such as potent antibacterial activity and efficient light absorption, make them highly attractive for combating bacterial infections and addressing environmental challenges. The incorporation of Cu further enhances their performance by synergistically augmenting the bactericidal and photocatalytic activities, making them key contenders in the discovery of newer materials for diverse applications, including healthcare, and wastewater treatment.

Declaration of Competing Interest

The author declares that she has no known competing financial interests or personal relationships that could have appeared to influence the work reported in this paper.

Acknowledgment

The author extends her gratitude to the Prince Sattam Bin Abdulaziz University for providing technical advice and facilities throughout this work.

References

- Ahmed, M.A., El-Katori, E.E., Gharni, Z.H., 2013. Photocatalytic degradation of methylene blue dye using Fe₂O₃/TiO₂ nanoparticles prepared by sol-gel method. *J. Alloy. Compd.* 553, 19–29. <https://doi.org/10.1016/j.jallcom.2012.10.038>.
- Ahmed, B., Hashmi, A., Khan, M.S., Musarrat, J., 2018. ROS mediated destruction of cell membrane, growth and biofilms of human bacterial pathogens by stable metallic AgNPs functionalized from bell pepper extract and quercetin. *Adv. Powder Technol.* 29, 1601–1616. <https://doi.org/10.1016/j.apt.2018.03.025>.
- Akhter, G., Khan, A., Ali, S.G., Khan, T.A., Siddiqi, K.S., Khan, H.M., 2020. Antibacterial and nematocidal properties of biosynthesized Cu nanoparticles using extract of holoparasitic plant. *SN Appl. Sci.* 2, 1–6. <https://doi.org/10.1007/s42452-020-3068-6>.
- Al-Enazi, N.M., Alsamhary, K., Ameen, F., Kha, M., 2023. Plant extract-mediated synthesis Cobalt doping in zinc oxide nanoparticles and their in vitro cytotoxicity and antibacterial performance. *Heliyon* 9. <https://doi.org/10.1016/j.heliyon.2023.e19659>.
- Ameen, F., 2022. Optimization of the synthesis of fungus-mediated Bi-metallic Ag-Cu nanoparticles. *Appl. Sci.* 12, 1384.
- Ameen, F., Alown, F., Al-Owaidi, M.F., Sivapriya, T., Ramirez-Coronel, A.A., Khat, M., Akhavan-Sigari, R., 2023a. African plant-mediated for biosynthesis silver nanoparticles and evaluation of their toxicity, and antimicrobial activities. *S. Afr. J. Bot.* 156, 213–222. <https://doi.org/10.1016/j.sajb.2023.03.010>.
- Ameen, F., Altuner, E.E., Elhoda Tiri, R.N., Gulbagca, F., Aygun, A., Sen, F., Majrashi, N., Orfali, R., Dragoi, E.N., 2023b. Highly active iron (II) oxide-zinc oxide

- nanocomposite synthesized *Thymus vulgaris* plant as bioreduction catalyst: Characterization, hydrogen evolution and photocatalytic degradation. *Int. J. Hydrogen Energy* 48, 21139–21151. <https://doi.org/10.1016/j.ijhydene.2022.11.229>.
- Ameen, F., Aygun, A., Seyrankaya, A., Elhouda Tiri, R.N., Gulbagca, F., Kaynak, İ., Majrashi, N., Orfali, R., Dragoi, E.N., Sen, F., 2023c. Photocatalytic investigation of textile dyes and *E. coli* bacteria from wastewater using Fe₃O₄@MnO₂ heterojunction and investigation for hydrogen generation on NaBH₄ hydrolysis. *Environ. Res.* 220, 115231 <https://doi.org/10.1016/j.envres.2023.115231>.
- Ameen, F., Majrashi, N., 2023. Recent trends in the use of cobalt ferrite nanoparticles as an antimicrobial agent for disability infections: A review. *Inorg. Chem. Commun.* 156, 111187 <https://doi.org/10.1016/j.inoche.2023.111187>.
- Ameen, F., Tiri, R.N.E., Bekmezci, M., Karimi, F., Bennini, N., Sen, F., 2023d. Microwave-assisted synthesis of Vulcan Carbon supported Palladium-Nickel (PdNi@VC) bimetallic nanoparticles, and investigation of antibacterial and Safranin dye removing effects. *Chemosphere* 339, 139630. <https://doi.org/10.1016/j.chemosphere.2023.139630>.
- Anandan, K., Rajendran, V., 2015. Effects of Mn on the magnetic and optical properties and photocatalytic activities of NiO nanoparticles synthesized via the simple precipitation process. *Mater. Sci. Eng. B: Solid-State Mater. Adv. Technol.* 199, 48–56. <https://doi.org/10.1016/j.mseb.2015.04.015>.
- Atmani, F., Bensmaili, A., Amrane, A., 2010. Methyl orange removal from aqueous solutions by natural and treated skin almonds. *Desalin. Water Treat.* 22, 174–181. <https://doi.org/10.5004/dwt.2010.1425>.
- Baker, S., Satish, S., 2012. International Journal of Bio-Inorganic Hybrid Nanomaterial Endophytes : Toward a vision in synthesis of nanoparticle for future therapeutic agents. *Int. J. Bio-Inorg. Hybrid Nanomater.* 1, 67–77.
- Banerjee, S., Show, B., Kundu, A., Ganguly, J., Gangopadhyay, U., Saha, H., Mukherjee, N., 2016. N-acetylcysteine assisted synthesis of core shell Ag₂S with enhanced light transmission and diminished reflectance: Surface modifier for c-SiNx solar cells. *J. Indus. Eng. Chem.* 40, 54–61. <https://doi.org/10.1016/j.jiec.2016.06.006>.
- Binjawhar, D.N., Al-Warhi, T., Siddiqui, G.A., Khan, A., 2023. Probing the interaction of zinc oxide nanorods with human serum albumin: A spectroscopic approach. *J. Biotechnol.* 362, 36–44. <https://doi.org/10.1016/j.jbiotec.2022.12.006>.
- Chauhan, R., Kumar, A., Pal Chaudhary, R., 2014. Photocatalytic degradation of methylene blue with Cu doped ZnS nanoparticles. *J. Lumines.* 145, 6–12. <https://doi.org/10.1016/j.jlumin.2013.07.005>.
- Elayaraja, M., Punithavathy, I.K., Jothibas, M., Muthuvel, A., Jeyakumar, S.J., 2020. Effect of rare-earth metal ion Ce³⁺ on the structural, optical and photocatalytic properties of CdO nanoparticles. *Nanotechnol. Environ. Eng.* 5, 25. <https://doi.org/10.1007/s41204-020-00091-z>.
- Fakhri, A., Pourmand, M., Khakpour, R., Behrouz, S., 2015. Structural, optical, photoluminescence and antibacterial properties of copper-doped silver sulfide nanoparticles. *J. Photochem. Photobiol. B: Biol.* 149, 78–83. <https://doi.org/10.1016/j.jphotobiol.2015.05.013>.
- Fernández, C., Larrechi, M.S., Callao, M.P., 2010. An analytical overview of processes for removing organic dyes from wastewater effluents. *TrAC - Trends Anal. Chem.* 29, 1202–1211. <https://doi.org/10.1016/j.trac.2010.07.011>.
- Hamed, M.S.G., Adedeji, M.A., Zhang, Y., Mola, G.T., 2020. Silver sulphide nanoparticles enhanced photo-current in polymer solar cells. *Appl. Phys. A* 126, 207. <https://doi.org/10.1007/s00339-020-3389-8>.
- Jesion, I., Skibniewski, M., Skibniewska, E., Strupiński, W., Szulc-Dąbrowska, L., Krajewska, A., Pasternak, I., Kowalczyk, P., Pińkowski, R., 2015. Graphene and carbon nanocompounds: Biofunctionalization and applications in tissue engineering. *Biotechnol. Biotechnol. Equip.* 29, 415–422. <https://doi.org/10.1080/13102818.2015.1009726>.
- Jyoti, K., Baunthiyal, M., Singh, A., 2016. Characterization of silver nanoparticles synthesized using *Urtica dioica* Linn. leaves and their synergistic effects with antibiotics. *J. Radiat. Res. Appl. Sci.* 9, 217–227. <https://doi.org/10.1016/j.jrras.2015.10.002>.
- Khan, A., Ameen, F., Khan, F., Al-Arfaj, A., Ahmed, B., 2020. Fabrication and antibacterial activity of nanoenhanced conjugate of silver (I) oxide with graphene oxide. *Mater. Today Commun.* 25, 101667 <https://doi.org/10.1016/j.mtcomm.2020.101667>.
- Khan, A., Kamal, T., Saad, M., Ameen, F., A. Bhat, S., Ahamad Khan, M., Rahman, F., 2023a. Synthesis and antibacterial activity of nanoenhanced conjugate of Ag-doped ZnO nanorods with graphene oxide. *Spectrochimica Acta - Part A: Molecular and Biomolecular Spectroscopy* 290, 122296. <https://doi.org/10.1016/j.saa.2022.122296>.
- Khan, A., Rahman, F., Nongjai, R., Asokan, K., 2021. Optical transmittance and electrical transport investigations of Fe-doped In₂O₃ thin films. *Appl. Phys. A Mater. Sci. Process.* 127, 1–11. <https://doi.org/10.1007/s00339-021-04490-0>.
- Khan, A., Saad, M., Kamal, T., Rahman, F., 2023b. Structural, morphological, optical and UV-light driven enhanced photocatalytic properties of Fe-doped NiO nanoparticles. *Mater. Chem. Phys.* 127923.
- Kumari, P., Chandran, P., Khan, S.S., 2014. Synthesis and characterization of silver sulfide nanoparticles for photocatalytic and antimicrobial applications. *J. Photochem. Photobiol. B: Biol.* 141, 235–240. <https://doi.org/10.1016/j.jphotobiol.2014.09.010>.
- Liu, T., Liu, B., Yang, L., Ma, X., Li, H., Yin, S., Sato, T., Sekino, T., Wang, Y., 2017. RGO/Ag₂S/TiO₂ ternary heterojunctions with highly enhanced UV-NIR photocatalytic activity and stability. *Appl. Catal. B: Environ.* 204, 593–601. <https://doi.org/10.1016/j.apcatb.2016.12.011>.
- Mittal, M., Sharma, M., Pandey, O.P., 2014. UV-Visible light induced photocatalytic studies of Cu doped ZnO nanoparticles prepared by co-precipitation method. *Sol. Energy* 110, 386–397. <https://doi.org/10.1016/j.solener.2014.09.026>.
- Okla, M.K., Janani, B., AL-ghamdi, A.A., Abdel-Maksoud, M.A., AbdElgawad, H., Das, A., Khan, S.S., 2022. Facile construction of 3D CdS-Ag₂S nanospheres: a combined study of visible light responsive photocatalysis, antibacterial and anti-biofilm activity. *Colloids and Surfaces A: Physicochemical and Engineering Aspects* 632, 127729. <https://doi.org/10.1016/j.colsurfa.2021.127729>.
- Pal, S., Tak, Y.K., Song, J.M., 2007. Does the antibacterial activity of silver nanoparticles depend on the shape of the nanoparticle? A study of the gram-negative bacterium *Escherichia coli*. *Appl. Environ. Microbiol.* 73, 1712–1720. <https://doi.org/10.1128/AEM.02218-06>.
- Pandurangan, M., Kim, D.H., 2015. In vitro toxicity of zinc oxide nanoparticles: a review. *J. Nanopart. Res.* 17, 158. <https://doi.org/10.1007/s11051-015-2958-9>.
- Parthipan, P., Cheng, L., Rajasekar, A., Govarthanan, M., Subramania, A., 2021. Biologically reduced graphene oxide as a green and easily available photocatalyst for degradation of organic dyes. *Environ. Res.* 196, 110983 <https://doi.org/10.1016/j.envres.2021.110983>.
- Pasukhun, N., Vinitnantharat, S., Gheewala, S., 2010. Investigation of decolorization of textile wastewater in an anaerobic/aerobic biological activated carbon system (A/A BAC). *Pak. J. Biol. Sci.* 13, 316–324. <https://doi.org/10.3923/pjbs.2010.316.324>.
- Perni, S., Hakala, V., Prokopovich, P., 2014. Biogenic synthesis of antimicrobial silver nanoparticles capped with l-cysteine. *Colloids Surf. A Physicochem. Eng. Asp.* 460, 219–224. <https://doi.org/10.1016/j.colsurfa.2013.09.034>.
- Podporska-Carroll, J., Myles, A., Quilty, B., McCormack, D.E., Fagan, R., Hinder, S.J., Dionysiou, D.D., Pillai, S.C., 2017. Antibacterial properties of F-doped ZnO visible light photocatalyst. *J. Hazard. Mater.* 324, 39–47. <https://doi.org/10.1016/j.jhazmat.2015.12.038>.
- Qian, X.F., Yin, J., Feng, S., Liu, S.H., Zhu, Z.K., 2001. Preparation and characterization of polyvinylpyrrolidone films containing silver sulfide nanoparticles. *J. Mater. Chem.* 11, 2504–2506. <https://doi.org/10.1039/b103708k>.
- Rajeshwar, K., Osugi, M.E., Chanmanee, W., Chenthamarakshan, C.R., Zanon, M.V.B., Kajitvichyanukul, P., Krishnan-Ayer, R., 2008. Heterogeneous photocatalytic treatment of organic dyes in air and aqueous media. *J. Photochem. Photobiol. C: Photochem. Rev.* 9, 171–192. <https://doi.org/10.1016/j.jphotochemrev.2008.09.001>.
- Sathishkumar, P., Preethi, J., Vijayan, R., Mohd Yusoff, A.R., Ameen, F., Suresh, S., Balagurunathan, R., Palvannan, T., 2016. Anti-acne, anti-dandruff and anti-breast cancer efficacy of green synthesised silver nanoparticles using *Coriandrum sativum* leaf extract. *J. Photochem. Photobiol. B: Biol.* 163, 69–76. <https://doi.org/10.1016/j.jphotobiol.2016.08.005>.
- Sawai, J., Yoshikawa, T., 2004. Quantitative evaluation of antifungal activity of metallic oxide powders (MgO, CaO and ZnO) by an indirect conductimetric assay. *J. Appl. Microbiol.* 96, 803–809. <https://doi.org/10.1111/j.1365-2672.2004.02234.x>.
- Stoimenov, P.K., Klingner, R.L., Marchin, G.L., Klabunde, K.J., 2002. Metal oxide nanoparticles as bactericidal agents. *Langmuir* 18, 6679–6686. <https://doi.org/10.1021/la0202374>.
- Tang, S., Zheng, J., 2018. Antibacterial activity of silver nanoparticles: Structural effects. *Adv. Healthc. Mater.* 7, 1701503. <https://doi.org/10.1002/adhm.201701503>.
- Thirumala Rao, G., Babu, B., Joyce Stella, R., Pushpa Manjari, V., Ravikumar, R.V.S.S.N., 2015. Spectral investigations on undoped and Cu²⁺ doped ZnO-CdS composite nanopowders. *Spectrochim. Acta - Part A: Mol. Biomol. Spectrosc.* 139, 86–93. <https://doi.org/10.1016/j.saa.2014.12.021>.
- Thirunavoukkarasu, M., Balaji, U., Behera, S., Panda, P.K., Mishra, B.K., 2013. Biosynthesis of silver nanoparticle from leaf extract of *Desmodium gangeticum* (L.) DC. and its biomedical potential. *Spectrochim. Acta - Part A: Mol. Biomol. Spectrosc.* 116, 424–427. <https://doi.org/10.1016/j.saa.2013.07.033>.
- Zhang, K.Z., Lin, B.Z., Chen, Y.L., Xu, B.H., Pian, X.T., Kuang, J.D., Li, B., 2011. Fe-doped and ZnO-pillared titanates as visible-light-driven photocatalysts. *J. Colloid Interface Sci.* 358, 360–368. <https://doi.org/10.1016/j.jcis.2011.03.021>.